Opt Quant Electron (2012) 44:255–263
DOI 10.1007/s11082-012-9543-6

Picosecond wavelength conversion using semiconductor optical amplifier integrated with microring resonator notch filter

M. Razaghi · M. Gandomkar · V. Ahmadi · N. K. Das · M. J. Connelly

Received: 30 September 2011 / Accepted: 5 January 2012 / Published online: 20 January 2012

Abstract In this paper, we analyse the picosecond wavelength conversion using semiconductor optical amplifier (SOA) with a novel technique. For an accurate and precise modelling, all the nonlinear effects that are relevant to picosecond and subpicosecond pulse regime, such as, self-phase modulation, nonlinear Kerr effect, spectral hole burning, carrier heating, carrier depletion, two-photon absorption and group velocity dispersion are taken into account in the SOA model. We integrate the structure with a microring resonator notch filter to eliminate the unwanted pump and probe signals at the output of the system. It shows that with the three coupled microring resonators, output four-wave mixing (FWM) signal generated by the SOA can be filtered accurately. Moreover, our results demonstrate that the microring resonator can be used for modifying the shape and spectrum of the output FWM signal. Simulation results show that this new technique enhances the output time bandwidth product.

Keywords Semiconductor optical amplifier · Microring resonators · Nonlinear effects · Four-wave mixing · Pulse shaping

M. Razaghi (✉)
Department of Electrical and Computer Engineering, University of Kurdistan, Sanandaj, Iran
e-mail: m.razaghi@uok.ac.ir

M. Gandomkar
Department of Electrical and Computer Engineering, Jondi-Shapour University of Technology, Dezful, Iran

V. Ahmadi
Department of Electrical and Computer Engineering, Tarbiat Modares University, Tehran, Iran

N. K. Das
Department of Electrical and Computer Engineering, Curtin University, Perth, WA 6845 Australia

M. J. Connelly
Department of Electronic and Computer Engineering, University of Limerick, Limerick, Ireland

1 Introduction

All optical wavelength converters are the important key elements in ultrafast optical communication systems (Meuer 2011; Connelly 2002). Among different schemes for high-speed wavelength conversion, using wave-mixing technique for generating four-wave mixing (FWM) signals in semiconductor optical amplifiers (SOAs) is important and a promising choice due to its inherent ultrafast nonlinearities (Das et al. 2000).

For the input pulsewidths of picoseconds, besides self-phase modulation (SPM), which has the dominant effects on propagated signal, other nonlinear phenomena, such as, ultrafast nonlinear refraction index (UNRI), spectral hole burning (SHB), carrier heating (CH), carrier depletion (CD), two photon absorption (TPA) and nonlinear Kerr effects change the characteristics of SOA's output signal shape and spectrum (Razaghi et al. 2009a). Therefore, all of these nonlinearities are included in our model. Based on the simulation time and accuracy of results, finite difference beam propagation method (FD-BPM) is used for modelling of the nonlinear wave propagation in the SOA, because of short convergence time and excellent accuracy of the results (Das et al. 2000).

In this paper, we propose a new technique to investigate (extract) the picosecond wavelength conversion using the SOA with microring resonator notch filters. In this new technique, high power input pump and probe signals are mixed together and the low power FWM and idler signals are generated. These signals have central frequencies close together and coexist at the output of the SOA. For the separation of this output FWM signal from the other signals, it requires a narrow band filter with a good side band rejection. For this purpose, we propose a microring based notch filter integrated with the SOA.

A simple schematic diagram of the proposed system is shown in Fig. 1. The wavelength converter consists of an SOA and an integrated passive microring resonator including the three microrings. Coupling between the microrings and straight waveguides is completed through a gap space between the waveguides. The coupling coefficients can be selected by designing (or controlling) the gap spaces. This structure can filter the output FWM signal of the SOA and suppress the high power pump and probe energy at the output of the system.

Up to now, there are different methods reported to reshape the output signals (Razaghi et al. 2009a,b). Based on the proposed scheme, it has also been shown that the microring resonator can reshape the FWM signal by reducing the side effects of SOA's nonlinearities. By this technique, output signal becomes more symmetric in comparison with the SOA's output FWM signal.

This paper is organized as follow: Sect. 1 is introduction, Sect. 2 is theory of the model, the equations which govern the dynamics of the amplification process, Sect. 3 is simulation results and discussion and finally the conclusions are in Sect. 4.

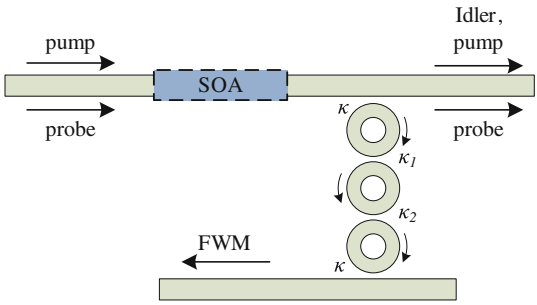

Fig. 1 Schematic diagram of the proposed wavelength convertor system

2 Theory of the model

To include all the important nonlinear effects in the SOA, the modified nonlinear Schrödinger equation (MNLSE) is used for this modeling (Das et al. 2000):

$$\left[\frac{\partial}{\partial z} - \frac{i}{2}\beta_2\frac{\partial^2}{\partial\tau^2} + \frac{\gamma}{2} + \left(\frac{\gamma_{2p}}{2} + ib_2\right)|V(z,\tau)|^2\right]V(z,\tau) \tag{1}$$
$$= \left\{\frac{1}{2}g_N(\tau)\left[\frac{1}{f(\tau)} + i\alpha_N\right] + \frac{1}{2}\Delta g_T(\tau)\,(1+i\alpha_T)\right.$$
$$\left. - i\frac{1}{2}\left.\frac{\partial g(\tau,\omega)}{\partial\omega}\right|_{\omega_0}\frac{\partial}{\partial\tau} - \frac{1}{4}\left.\frac{\partial^2 g(\tau,\omega)}{\partial\omega^2}\right|_{\omega_0}\frac{\partial^2}{\partial\tau^2}\right\}V(z,\tau)$$

where, $V(z,\tau)$ is the complex envelope function of an optical pulse. The definitions of some parameters in the Eq. (1) are as follows:

$$g_N(\tau) = g_0\exp\left[-\frac{1}{E_{sat}}\int_{-\infty}^{+\infty}u(s)\,|V(\tau-s)|^2\,ds\right] \tag{2}$$

$$f(\tau) = 1 + \frac{1}{\tau_{shb}P_{shb}}\int_{-\infty}^{\infty}u(s)\,e^{-s/\tau_{shb}}\,|V(\tau-s)|^2 ds \tag{3}$$

$$\Delta g_T(\tau) = -h_1\int_{-\infty}^{+\infty}u(s)e^{-s/\tau_{ch}}\times(1-e^{-s/\tau_{shb}})\,|V(\tau-s)|^2\,ds$$
$$-\mathrm{h}_2\int_{-\infty}^{+\infty}u(s)e^{-s/\tau_{ch}}\times(1-e^{-s/\tau_{shb}})\,|V(\tau-s)|^4\,ds \tag{4}$$

$$\left.\frac{\partial g(\tau,\omega)}{\partial\omega}\right|_{\omega_0} = A_1 + B_1\,[g_0 - g(\tau,\omega_0)] \tag{5}$$

$$\left.\frac{\partial^2 g(\tau,\omega)}{\partial\omega^2}\right|_{\omega_0} = A_2 + B_2\,[g_0 - g(\tau,\omega_0)] \tag{6}$$

$$g(\tau,\omega_0) = g_N(\tau,\omega_0)/f(\tau) + \Delta g_T(\tau,\omega_0) \tag{7}$$

where, $\tau = t - z/v_g$ is the frame of local time which propagates with the group velocity v_g of the optical pulse at central angular frequency $\omega_0(=2\pi f_0)$.

The slowly varying envelope function approximation is used in Eq. (1), where the temporal change of the complex envelope function is very slow compared with the cycle of an optical field. $|V(z,\tau)|^2$ represents the optical power of an optical pulse, β_2 is the group velocity dispersion (GVD), γ is linear loss, γ_{2p} is the two-photon absorption coefficient, $b_2(=\omega_0 n_2/cA)$ is the instantaneous self-phase modulation term due to the Kerr effect, n_2 is an instantaneous nonlinear refractive index, c is the velocity of light in vacuum, $A\ (=wd/\Gamma)$ is the effective area, d and w are the thickness and width of the active region, respectively, and Γ is the confinement factor.

In addition, $g_N(\tau)$ is the saturated gain due to carrier depletion, g_0 is the linear gain, E_{sat} is the saturation energy, τ_s is the carrier lifetime, $f(\tau)$ is the spectral hole-burning function, P_{shb} is the spectral hole-burning saturation power, τ_{shb} is the spectral hole-burning relaxation time, α_N and α_T are the linewidth enhancement factor associated with the gain changes

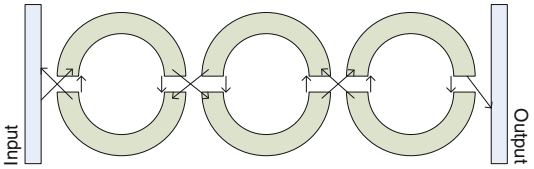

Fig. 2 Simulation of wave propagation in microrings by splitting the periphery at coupling points

due to the carrier depletion and carrier heating, respectively. $\Delta g_T(\tau)$ is the resulting gain change due to the carrier heating and two-photon absorption, $u(s)$ is the unit step function, τ_{ch} is the carrier heating relaxation time, h_1 is the contribution of stimulated emission and free-carrier absorption to the carrier heating gain reduction, and h_2 is the contribution of two-photon absorption. Finally, A_1 and A_2 are the slope and the curvature of the linear gain at ω_0, respectively, while B_1 and B_2 are constants describing the changes in these quantities with saturation (Das et al. 2000).

For solving Eq. (1), the SOA cavity is divided into M equal sections. By using a central-difference approximation in time domain and trapezoidal integration over spatial section, and applying an iterative procedure, a set of MNLSEs are solved with high precision in few seconds (Das et al. 2000).

Wave propagation equation in microrings is simulated utilizing 1D finite-difference time domain method (FDTD). This equation in the simplest form is (Gandomkar and Ahmadi 2011)

$$\left(\frac{1}{v_g}\frac{\partial}{\partial_t}+\frac{\partial}{\partial_z}\right)V(z,t)=0 \tag{8}$$

where, v_g is the group velocity and its value is 80 μm/ps. Periphery of the microrings is split at the coupling points, as shown in Fig. 2, and the wave propagation is solved in each half ring separately. At the coupling points, each traveling field is divided into two fractions as explained by arrows in Fig. 2. One part is coupled into the other waveguide with the rational coefficient $i\kappa'$, where i is the complex number and shows $\pi/2$ phase shift during the coupling and κ' is the coupling coefficient. The other part of the field remains in the waveguide with the rational coefficient σ' so that always $\kappa'^2+\sigma'^2=1$ (Gandomkar and Ahmadi 2011; Little et al. 1997). Here, σ' is transmission coefficient. On the other hand, input field of each half ring consists of a transmitted part and a coupled part. After traveling half of the periphery of the ring (length between the coupling points), an additional phase $2\pi^2 n_{eff} R/\lambda_0$ is added to $V(z,t)$ where λ_0 is the central wavelength of optical signal pulse.

3 Results and discussion

In simulation, we used the parameters of a bulk SOA (AlGaAs/GaAs, double heterostructure) with a wavelength of 0.86 μm. The parameters are listed in Table 1 (Razaghi et al. 2009a). The shape of the input signal is sech ^{2} and it is Fourier transform limited. The pulse duration of input signal is varied from 5 to 20 ps. The input probe energies are varied 0.2–1.6 pJ. The input pump pulse energy is 10 times stronger than the input probe pulse energy. The detuning frequency between the input pump and probe pulse is 1 THz. The applicability and precision of the SOA model have been validated through comparison with the earlier published results (Razaghi et al. 2009a).

The coupling coefficients between the waveguides are selected to realize a maximum flat bandpass filter. This means that it satisfies the condition $\kappa_1^2=\kappa_2^2=0.125\kappa^4$ (Little et al.

Table 1 List of parameters used in simulation Razaghi et al. (2009a)

Symbol	Quantity	Value
L	SOA length	$500\,\mu\text{m}$
A_r	Effective area	$5\,\mu\text{m}^2$
f_o	Center frequency of the pulse	349 THz
β_2	Group velocity dispersion	$0.05\,\text{ps}^2\,\text{cm}^{-1}$
E_{sat}	Saturation energy	80 pJ
α_N	Linewidth enhancement factor due to the carrier depletion	3.1
α_r	Linewidth enhancement factor due to the carrier heating	2.0
h_1	The contribution of stimulated emission and free carrier absorption to the carrier heating gain reduction	$0.13\,\text{cm}^{-1}\,\text{pJ}^{-1}$
h_2	The contribution of two photon absorption	$126\,\text{fs}\,\text{cm}^{-1}\,\text{pJ}^{-2}$
τ_s	Carrier lifetime	200 ps
τ_{ch}	Carrier heating relaxation time	700 fs
τ_{shb}	Spectral -hole burning relaxation time	60 fs
P_{shb}	Spectral -hole burning relaxation power	28.3 W
γ	Linear loss	$11.5\ \text{cm}^{-1}$
n_2	Instantaneous nonlinear Kerr effect	$-0.70\,\text{cm}^2\,\text{TW}^{-1}$
γ_{2p}	Two photon absorption coefficient	$1.1\,\text{cm}^{-1}\,\text{W}^{-1}$
A_1		$0.15\text{fs}\,\mu\text{m}^{-1}$
A_2	Parameters describing second order Taylor	-80 fs
B_1	expansion of the dynamically gain spectrum	$-60\,\text{fs}^2\,\mu\text{m}^{-1}$
B_2		$0\,\text{fs}^2$

1997) where, κ_1 and κ_2 are the coupling coefficients between the two microrings and κ is the coupling coefficient between each straight waveguide and its nearby microring. Here, κ= 0.3 [where, it is approximately unchanged in our filtering window (Hagness 1998)] and radii of microrings are $R = 2.5\ \mu$m. The effective refractive index of the ring waveguide is $n_{eff} = 3$.

The plot as shown in Fig. 3, compares the ability of single, double and triple microring structures in extraction of the FWM signal from the SOA output. Here, we can see that the single and double microring structures cannot make a sufficient out-of-band rejection and the FWM signal cannot be filtered effectively. Therefore, to filter out all of the signals except the FWM signal, three microrings are cascaded (as shown in Fig. 1). This provides the required out-of-band signal rejection (80 dB reduction of output pump signal) to eliminate the amplified pump energy from the output of the SOA.

The output FWM signal spectra of both the SOA and microring are shown in Fig. 4, for the input probe signal energy of 1.6 pJ and pulsewidth of 5 ps. As it is depicted, the microring's output FWM signal spectral width is decreased, because of the narrow band filter imposed by the microring structure. Besides, the oscillatory phenomena, which are due to SOA nonlinearities, are removed from the FWM spectrum by this technique. As a result, the output FWM signal shape and spectrum of the microring are more symmetric in comparison with SOA's output FWM signal.

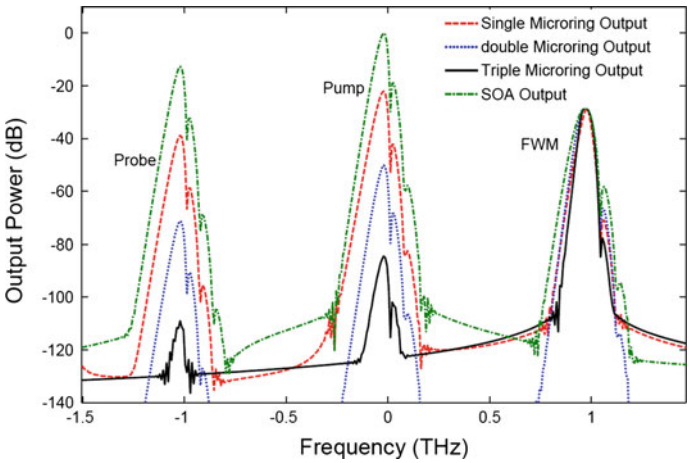

Fig. 3 Comparison among the output signal of single, double and triple microring structures. Here, the probe energy is 0.8 pJ and pulse duration is 10 ps

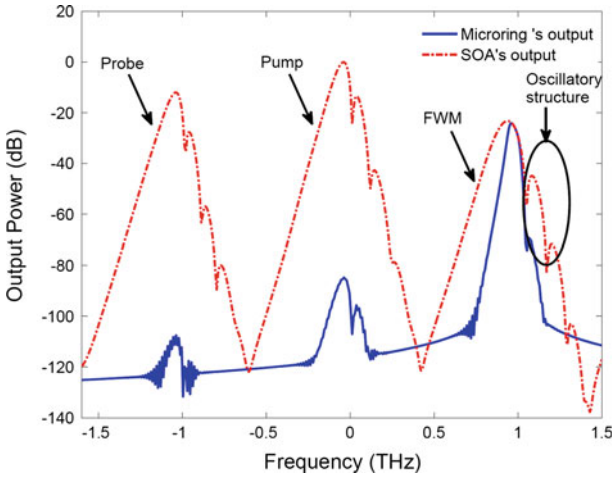

Fig. 4 Output spectra of the SOA and the triple microring structure

Figure 5 shows the output FWM signal shape of the SOA and microring corresponding to the Fig. 4. Based on these results, it is clear that the microring can perfectly filter the FWM signal. To compare the results of a ring resonator notch filter with SOA's FWM signal, we filtered the output spectrum of Fig. 4 from −500 GHz to +500 GHz of the FWM signal's central frequency (+1 THZ) and performed the inverse Fourier transform of the respective components. As it is illustrated, the microring structure suppresses the SOA's nonlinearities and makes the FWM signal more symmetric. In addition, the time bandwidth product (TBP) of the SOA's output FWM signal decreases from 0.5 to 0.45 in microring's output FWM signal.

Figure 6 depicts the output spectral width of both the FWM signal of SOA and the microring for different input pulsewidths and energies. As the microring notch filter's bandwidth is 50 GHz, the FWM signal spectrum is compressed to more than half of SOA's output FWM signal for typical cases. This improves the TBP of the filtered FWM signal. For signals

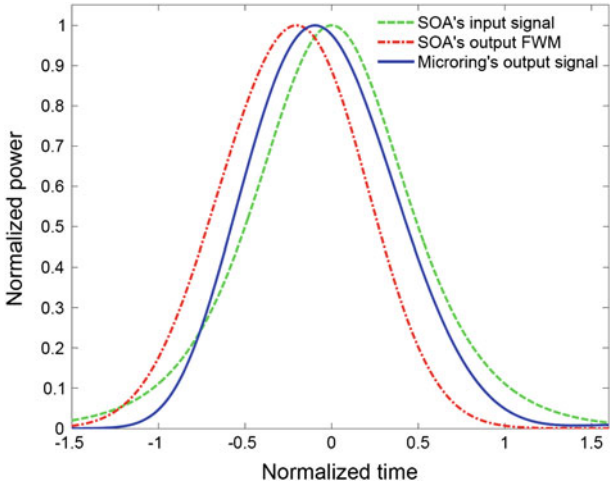

Fig. 5 Temporal output signal power of SOA and microring versus normalized time characteristics. The time scale is normalized to the pulsewidth of each corresponding signal

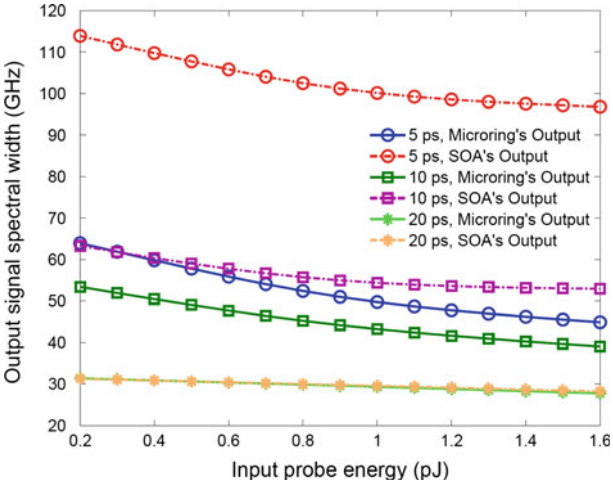

Fig. 6 Output signal spectral width of SOA's and microring's versus the input probe energy characteristics for different input pulsewidths

having larger pulsewidths, taking into account that signal frequency spectral width is reduced and microring filter spectral width remains unchanged, the effect of microring on spectral characteristics of FWM signal is decreased, although the filtering mechanism works perfectly.

The output FWM signal peak shift and output FWM signal energy of SOA and the microring for different input pulsewidths and energies are shown in Fig. 7. Based on the simulation results, the output FWM signal's peak shift (Fig. 7a) is decreased by the proposed new scheme. As it is shown in Fig. 4, the SOA's output FWM signal spectrum is distorted due to the nonlinearities of SOA's (i.e., SOA's medium nonlinearities). Therefore, using the microring notch filter the output FWM signal power is reduced as shown in Fig. 7b. Consequently, the effect of nonlinearities due to the high energy input pulses can be decreased in our new

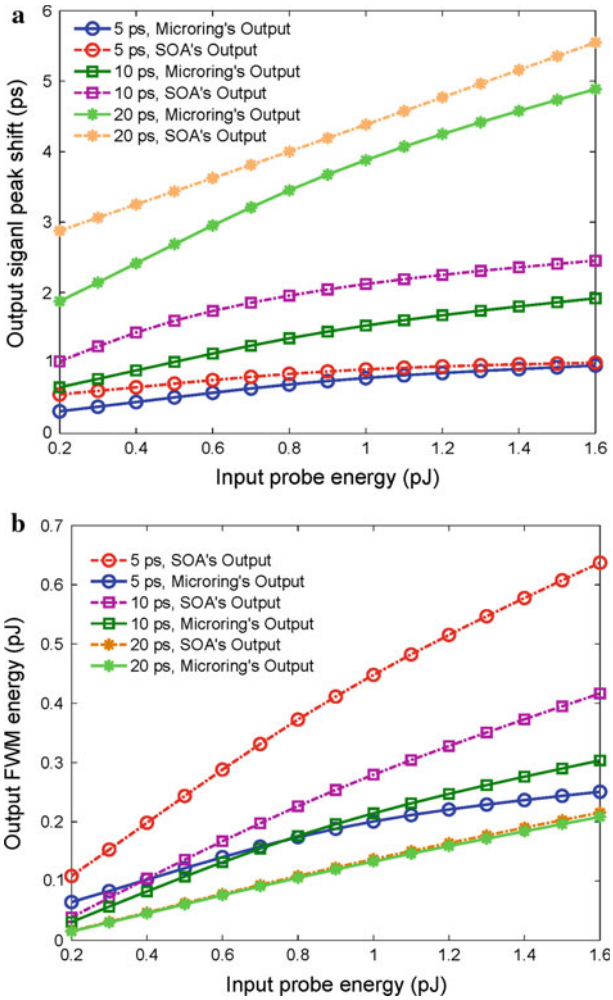

Fig. 7 Peak shift **a** and energy **b** of FWM signal at the output of SOA and microring for different input pulsewidths versus input probe energy characteristics

scheme and the microring's output becomes more symmetric. It should be noted that for shorter input probe signals (that has the broader/wider spectrum), the effect of microring filter on the output FWM signal energy becomes more noticeable. But in this case, the SOA's output FWM signal is affected by not only the SPM effect, but also by the fast process of nonlinear phenomena (Das et al. 2000; Razaghi et al. 2009a). Therefore, although the FWM output signal power is suppressed considerably, the influence of the microring filter on the output FWM signal symmetry becomes negligible.

4 Conclusion

We have numerically modelled the picosecond wavelength conversion using SOA integrated with microring notch filter. We used three cascaded microrings to provide the required quality

factor and the sideband rejection to separate the FWM signal from high power pump and probe signals at very close frequencies. The simulation result has shown that the microring resonator, in addition to filtering of the FWM signal, enhances its temporal signal shape symmetry. It has also shown that the output FWM signal spectrum of the microring is more symmetric in comparison with the output FWM signal of SOA. The microring structure suppressed the SOA's nonlinearities and the FWM signal became more symmetric. From the simulated results, we observed that the microring is useful and it can filter the FWM signal perfectly. In addition, the TBP of the SOA's output FWM signal decreases from 0.5 to 0.45 in microring's output FWM signal. Finally, we conclude that the microring has advantages than other methods and it leads to the compression of FWM signal spectral widths.

References

Connelly, M.J.: Semiconductor Optical Amplifiers. Kluwer, Boston, MA (2002)

Das, N.K., Yamayoshi, Y., Kawaguchi, H.: Analysis of basic four-wave mixing characteristics in a semiconductor optical amplifier by the finite-difference beam propagation method. IEEE J. Quantum Electron. **36**(10), 1184–1192 (2000)

Gandomkar, M., Ahmadi, V.: Design and analysis of enhanced second harmonic generation in AlGaAs/AlO_x microring waveguide. Opt. Express **19**, 9408–9418 (2011)

Hagness, H.C.: FDTD computational electromagnetics modeling of microcavity lasers and resonant optical structures. PhD thesis Dissertation, Illinois, USA, Northwestern University (1998)

Little, B.E., Chu, S.T., Haus, H.A., Foresi, J., Laine, J.P.: Microring resonator channel dropping filters. J. Lightw. Technol. **15**, 998–1005 (1997)

Meuer, C. et al.: 80 Gb/s wavelength conversion using a quantum-dot semiconductor optical amplifier and optical filtering. Opt. Express **19**, 5134–5142 (2011)

Razaghi, M., Ahmadi, V., Connelly, M.J.: Comprehensive finite-difference time-dependent beam propagation model of counterpropagating picosecond pulses in a semiconductor optical amplifier. IEEE/OSA J. Lightw. Technol. **27**(15), 3162–3174 (2009)

Razaghi, M., Ahmadi, V., Connelly, M.J.: Femtosecond pulse shaping using counter-propagating pulses in a semiconductor optical amplifier. Opt. Quantum Electron. (Springer) **41**, 513–523 (2009)